Combined Density Functional Theory and Interatomic Potential Study of the Bulk and Surface Structures and Properties of the Iron Sulfide Mackinawite (FeS)

ARTICLE *in* THE JOURNAL OF PHYSICAL CHEMISTRY C · APRIL 2008

Impact Factor: 4.77 · DOI: 10.1021/Jp8001959

3 AUTHORS, INCLUDING:

Ricardo Grau-Crespo
University of Reading
72 PUBLICATIONS **772** CITATIONS
SEE PROFILE

Nora H. de Leeuw
Cardiff University
240 PUBLICATIONS **4,431** CITATIONS
SEE PROFILE

Combined Density Functional Theory and Interatomic Potential Study of the Bulk and Surface Structures and Properties of the Iron Sulfide Mackinawite (FeS)

A. J. Devey,* R. Grau-Crespo, and N. H. de Leeuw

Department of Chemistry, University College, University of London, 20 Gordon Street, London, WC1H 0AJ, United Kingdom

Received: January 9, 2008; Revised Manuscript Received: April 10, 2008

The iron sulfide mackinawite (FeS) is modeled by density functional theory calculations, the results of which are used to derive a set of interatomic potentials for this material. We have investigated the effect of adding a Hubbard U_{eff} term to the gradient-corrected (GGA) functional, but whereas good agreement is shown with experimental data when pure GGA ($U_{\text{eff}} = 0$) is employed, for values of U_{eff} greater than zero the solution becomes unphysical, an indication that the Fe valence electrons within mackinawite are delocalized. This property is further evidenced by the density of states, which confirms a metallic nature from delocalization of the Fe d orbital at all U_{eff} values. Mackinawite is calculated to be a nonmagnetic material, in accord with experiment. We have also derived a set of interatomic potentials by fitting to observables including geometry, phonon frequencies, and elastic constants, which were calculated for isolated mackinawite layers using DFT. The derived potential model is used to calculate the unrelaxed and relaxed structures and energies for the {100}, {010}, {001}, {110}, {101}, {011}, and {111} surfaces of mackinawite. The {001} surface, terminating at S atoms, with a calculated surface energy of 0.07 J m^{-2}, is found to be the most stable surface with very little surface relaxation compared to the bulk material.

1. Introduction

Mackinawite, often referred to as tetrahedral FeS, is composed of FeS layers with Fe sandwiched between S sheets, which are held together by weak van der Waals interactions.[1] It is the first iron sulfide to form in most ambient environments[2] and is also produced by certain types of bacteria.[3] Mackinawite has been implicated in many important processes, particularly in its ability to capture heavy metal atoms within vacancy sites between layers[4] and in the development of prebiotic metabolism.[5] Naturally occurring mackinawite is often reported as nonstoichiometric,[6] resulting from a sulfur deficiency, and as such its formula is conventionally written as FeS_{1-x} (typically $0 < x < 0.07$). However, synthetic mackinawite is close to the stoichiometric material.[7]

The structure of mackinawite is now well-known (Figure 1) with space group *P4nmm* (no. 129)[8] and a tetragonal unit cell with parameters $a = b = 3.674$ Å and $c = 5.033$ Å.[9] Sulfur atoms are tetrahedrally coordinated in relation to a basal plane of iron atoms. A number of experimental studies have reported the properties of mackinawite, including its phase transition to greigite[10,11] and also pyrrhotite,[9] its surface chemistry,[2] and its thermodynamic stability.[12] Mössbauer effect spectroscopy measurements have confirmed the absence of any magnetic moment.[6] There has been some confusion concerning the conductive nature of mackinawite, with Bertaut et al.[1] claiming nonmetallic behavior. However, the absence of any magnetic moment and the close Fe−Fe distance (2.65 Å) within each layer indicate that there is likely to be extensive Fe d orbital delocalization and associated metallic behavior in the basal plane.[6,9] The high reactivity of mackinawite toward oxygen has resulted in little being known about the physical characteristics of this material, in particular its elastic behavior.

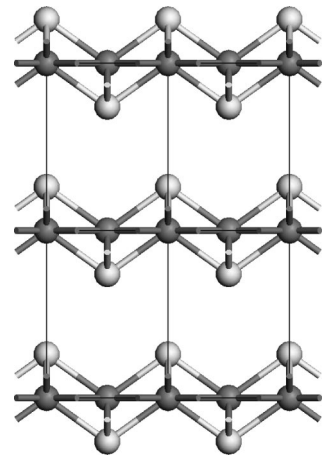

Figure 1. Structure of mackinawite, viewed along the *a*-axis. (Fe is shown in black, S in white with shading.)

Computational studies of the iron sulfides have tended to focus upon pyrite, e.g., refs 13 and 14. The approximate linear muffin tin orbital method used by Welz and Rosenberg[15] is the only instance of a computational study into the electronic structure of FeS tetrahedra. However, this study dealt exclusively with isolated FeS_4 tetrahedra with corner-sharing units, whereas mackinawite is actually composed of edge-sharing, slightly distorted tetrahedra.[16] A study of mackinawite using modern quantum mechanical techniques is clearly desirable. In this paper, density functional theory (DFT) calculations of the mackinawite structure are performed in order to investigate the electronic structure and magnetic behavior of this material. We also calculate the elastic constants and phonon frequencies of isolated mackinawite layers, and we use this information to derive a set of classical interatomic potential parameters for mackinawite. A successful interatomic potential model for

* Corresponding author. E-mail: a.devey@ucl.ac.uk.

10.1021/jp8001959 CCC: $40.75
Published on Web 06/25/2008

mackinawite facilitates the future analysis of a number of interesting properties of this important mineral, for example, defect behavior, surface properties, and crystal growth processes. The latter part of this paper examines the unrelaxed and relaxed surface energies of the {100}, {010}, {001}, {110}, {101}, {011}, and {111} surfaces and the displacement of surface atoms upon energy minimization. Calculations using the derived potential model reveal that the {001} surface is by far the most stable, making it the dominant surface in the morphology of mackinawite crystals.

2. Methodology

2.1. DFT Calculations. The mackinawite structure is modeled using the Vienna ab initio simulation program (VASP),[17–20] which utilizes spin-polarized DFT with a basis set of plane waves. The theory and application of the plane−wave DFT methodology have been extensively reviewed elsewhere;[21] it is well-established and has been applied to a wide range of materials including metal sulfides,[22–24] oxides,[25–27] and the bulk and surfaces of metals.[28] All calculations were performed within the generalized gradient approximation (GGA), using the exchange-correlation functional developed by Perdew et al.[29] and the spin interpolation formula of Vosko et al.[30] The interaction between the valence electrons and the core was described with the projected augmented wave (PAW) method[31] in the implementation of Kresse and Joubert.[32] The core levels, which were kept frozen during the calculations, consisted of orbitals up to, and including, the 3p levels for Fe and the 1p level for sulfur. All calculations were performed with an energy cutoff of 400 eV and a Monkhorst−Pack (MP)[33] grid of 11 × 11 × 11. In order to improve the convergence of the Brillouin zone integrations, the partial occupancies were determined using Gaussian smearing, with a set width for all calculations of 0.02 eV. These smearing techniques can be considered in the form of a finite-temperature DFT[34] where the variational quantity is the electronic free energy. The optimization of the structures was conducted via a conjugate gradients technique, which utilizes the total energy and the Hellmann−Feynman forces on the atoms.

We have also performed calculations using the so-called GGA+U method, in the simple formulation by Liechtenstein et al.[35] and Dudarev et al.,[36] where a single parameter, U_{eff}, determines an orbital-dependent correction to the GGA energy:

$$E_{\mathrm{GGA+U}} = E_{\mathrm{GGA}} + U_{\mathrm{eff}} \sum_{\sigma} Tr[\rho^{\sigma} - \rho^{\sigma}\rho^{\sigma}]$$

where ρ^{σ} is the on-site density matrix with spin component σ. The parameter U_{eff} is generally expressed as the difference between two parameters, the Hubbard U_{eff}, which is the Coulomb-energetic cost to place two electrons at the same site, and an approximation of the Stoner exchange parameter I, which is almost constant at ∼1 eV.[37] The GGA+U correction alters the one-electron potential locally for the specified orbitals of the metal atoms (here the Fe d orbitals), reducing the hybridization with the ligands (here the S atoms). The $U_{eff} = 0$ case represents the GGA limit. Details of the implementation of the DFT+U method in the VASP code can be found in the work by Rohrbach et al.,[23] where it was also shown that the introduction of the Hubbard correction improves the description of many transition metal sulfides.

2.2. Interatomic Potential Calculation Methodology. GULP is a molecular modeling program which is used extensively for the derivation of interatomic potential parameters.[38] The interatomic potential description of a material utilizes the Born model of solids,[39] which assumes that the ions in the crystal lattice interact via long- and short-range electrostatic forces. Such simulations provide a powerful technique for modeling crystal structures and physical processes such as defect and adsorption behavior. Parameter fitting uses the "sum of squares" method to measure the quality of the fit. The method may be defined as

$$F = \sum_{\mathrm{allobservables}} W(f_{\mathrm{calc}} - f_{\mathrm{obs}})^2$$

where f_{calc} is the calculated quantity, f_{obs} is the observed quantity, and W is a weighting factor. The aim of the fit is to minimize the sum of squares (ideally to zero) by varying the potential parameters until a suitable fit is found.

The short-range forces, which include both the repulsions and the van der Waals attraction between neighboring electron charge clouds, are expressed by simple analytical functions. In this case the short-range interactions between the iron and sulfur atoms are described using an effective Buckingham potential:

$$\Phi_{ij}(r_{ij}) = A_{ij} e^{-r_{ij}/\rho_{ij}} - \frac{C_{ij}}{r_{ij}^6}$$

In the classical picture of the atom, A_{ij} and ρ_{ij} are the size and hardness of the ion, respectively. However in an effective pair potential such as this, the A_{ij} and ρ_{ij} parameters have become interdependent. Thus, the first term represents the short-range repulsive interaction between the ions, whereas the second term represents the attractive van der Waals forces (also known as dispersive forces). The electronic polarizability of the sulfur ion is accounted for via the shell model of Dick and Overhausen[40] in which each polarizable ion is represented by a core and a massless shell, connected by a theoretical "spring" and an associated spring constant. The polarizability of the model ion is then determined by the spring constant and the charges of the core and shell. The core and shell of the same atom interact via a harmonic potential:

$$\Phi_{ij}^{\mathrm{core-shell}}(r_{ij}) = \frac{1}{2} K_{ij}(r_{ij} - r_0)^2$$

where K_{ij} is the bond force constant, r_{ij} is the separation between the core and shell centers, and r_0 the separation at equilibrium.

2.3. Surface Energy Calculation Methodology. The computer code METADISE[41] was used to perform simulations on the FeS surfaces. This scheme treats the crystal as planes of atoms, which are periodic in two dimensions. Surfaces are modeled by considering a single block, extending down from the surface of the crystal into the bulk. The simulation is initiated by dividing this block into two regions, 1 and 2. Region 1 is the *near-surface region*, which is composed of atoms adjacent to the surface. Region 2 is the *bulk region* and is composed of bulk atoms. The ions in region 1 are allowed to relax to their minimum energy configuration, whereas the ions of region 2 are fixed at their bulk equilibrium positions. All calculations were carried out on fully converged region sizes.

The surface energy is defined as the energy per unit area required to form the crystal surface relative to the bulk. The surface energy (γ) is therefore given by

$$\gamma = \frac{U_{\mathrm{s}} - U_{\mathrm{b}}}{A}$$

where U_{s} represents the energies of region 1, U_{b} represents the energy of an equivalent region of bulk atoms, and A is the surface area.

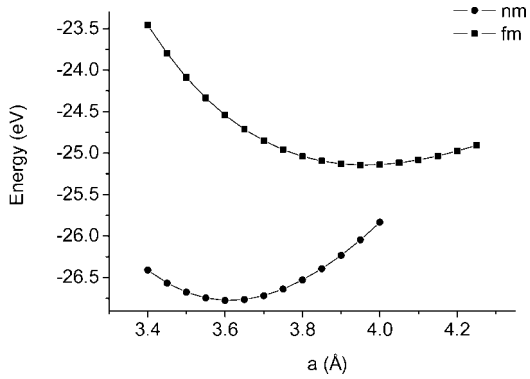

Figure 2. Graph of the variation of the total energy with *a* parameter for mackinawite (*c* parameter kept fixed) at $U_{eff} = 0$ eV.

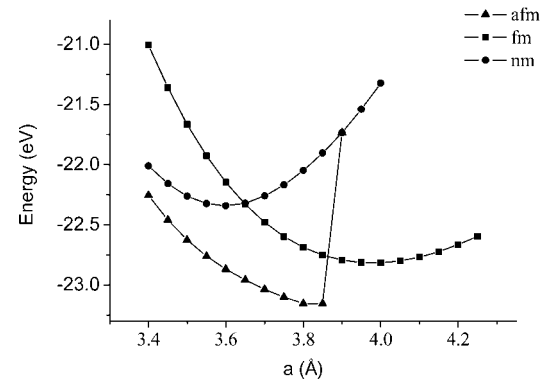

Figure 3. Graph of the variation of the total energy with *a* parameter for mackinawite (*c* parameter kept fixed) at $U_{eff} = 2$ eV.

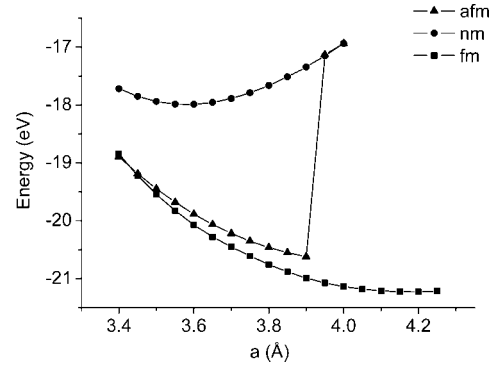

Figure 4. Graph of the variation of the total energy with *a* parameter for mackinawite (*c* parameter kept fixed) at $U_{eff} = 4$ eV.

Tasker[42] identified the existence of three types of surfaces. Type I surfaces comprise stoichiometric layers and possess no dipole normal to the surface. Type II surfaces are composed of units repeated over one or more layers, with no overall dipole. Type III surfaces cannot be cleaved without producing a dipole. A requirement for this calculation is that the unit cell must not possess a dipole perpendicular to the surface, as this dipole when repeated throughout the crystal results in divergence of the surface energy[43] and dipolar surfaces do not exist experimentally. Thus, any type III surfaces must be reconstructed into type I or II. Not all surfaces of a given orientation are equivalent, and in many cases there exist more than one nonidentical repeat unit for a particular (*hkl*) surface. Crystal morphologies are predicted from surface energies using Wulff's theorem[44] in which the equilibrium form of a crystal for a given volume possesses minimum total surface energy. Thus, the morphological significance of a crystal surface is determined by its surface energy.

3. Results

3.1. DFT Calculations. In order to investigate the mackinawite structure using DFT, calculations are performed for each of three magnetic arrangements: ferromagnetic, nonmagnetic, and antiferromagnetic. The non-magnetic case corresponds to a non spin-polarized solution, where all iron present in the structure is in the low spin state. The ferromagnetic arrangement corresponds to spin-polarized iron ions with the magnetic moments oriented in the same direction, and the antiferromagnetic case corresponds to neighboring iron ions oriented in antiparallel directions. In addition, each system is calculated with values of $U_{eff} = 0$, 2, and 4 eV.

In order to establish the structures predicted for each of these cases, the lattice energies for a range of values of the *a* parameter (and equivalent *b* parameter to satisfy structural symmetry) are calculated in order to determine each minimum. We chose the range of *a* to be between 3.4 and 4.25 Å to ensure that if possible all local energy minima are observed, with steps of 0.05 Å between points. The *c* parameter was initially fixed at the experimentally determined value of 5.033 Å.

The graph in Figure 2 shows the VASP results for $U_{eff} = 0$ eV, where the lines correspond to a parabolic fit to each set of data. This plot demonstrates that the lowest energy and thus most stable state for $U_{eff} = 0$ eV is clearly the nonmagnetic arrangement. The minimum energy of the nonmagnetic structure corresponds to an *a* parameter of 3.612 Å, compared to the experimentally reported measurement of 3.674 Å. The ferromagnetic solution gives an equilibrium lattice parameter *a* of nearly 4 Å, indicating an increase of about 10% compared to the experimental value. The mackinawite structure is unable to support an antiferromagnetic structure which collapses into the nonmagnetic arrangement.

TABLE 1: Energy Minimum Location for Each of the Magnetic Structures for the $U_{eff} = 0$, 2, and 4 eV Calculations

	$U = 0$ eV		$U = 2$ eV		$U = 4$ eV	
	FM	NM	FM	NM	FM	NM
E (eV)	−25.145	−26.775	−22.817	−22.339	−21.231	−17.991
a (Å)	3.972	3.612	3.988	3.597	4.209	3.580

Figure 3 demonstrates that for the case of $U_{eff} = 2$ eV, the nonmagnetic case is no longer the most stable. Instead, the antiferromagnetic arrangement possesses the lowest energy. However, at a lattice parameter value of 3.9 Å and above, this arrangement cannot be supported, and it collapses to the nonmagnetic case, similarly to the $U_{eff} = 0$ eV case. The ferromagnetic case predicts a very large lattice parameter compared to experiment. With increasing U_{eff}, the nonmagnetic case shows very little variation in the position of its energy minimum as a function of the *a* parameter.

Figure 4 shows the VASP calculations for $U_{eff} = 4$ eV. The increase in the stability of the ferromagnetic case is evident, and a large increase in its predicted *a* parameter suggests that the increasing electron correlation causes increased stability for this arrangement. As in the $U_{eff} = 2$ eV case, the structure is unable to support an antiferromagnetic arrangement for $a >$ 3.9 Å. The nonmagnetic arrangement has a much higher energy minimum than the ferromagnetic case, and Table 1 shows the calculated *a* parameters at the minimum internal energies for each of the three magnetic cases and U_{eff} values considered.

The inability of the mackinawite structure to support a stable antiferromagnetic arrangement over a reasonable range of *a*

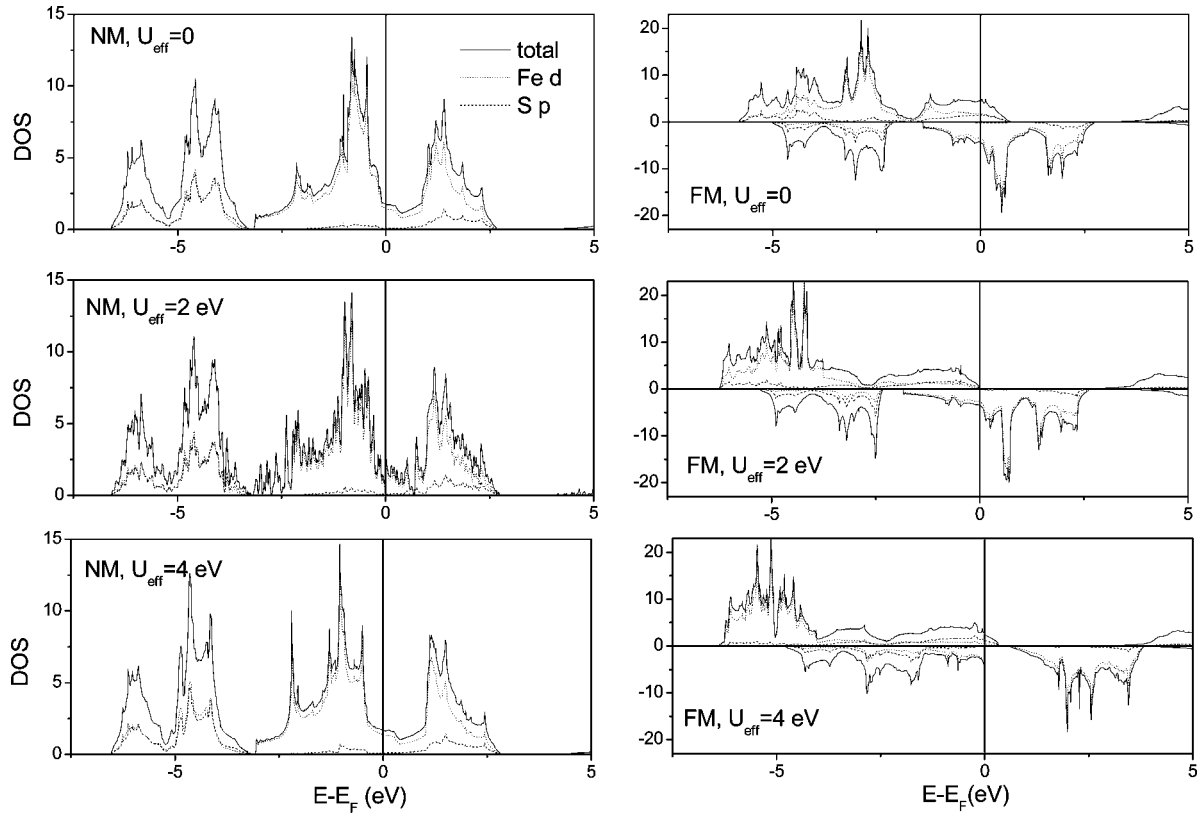

Figure 5. DOS graphs for nonmagnetic and ferromagnetic conditions for each U_{eff} value at $T = 0$ K. Each graph shows the total DOS and the contributions from the iron d orbitals and the sulfur p orbitals. The DOS is in units of "number of states per unit cell".

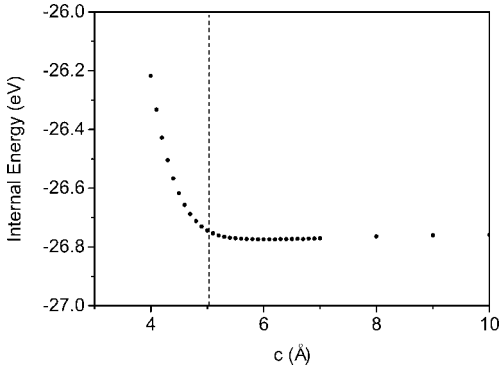

Figure 6. Variation of internal energy with c parameter for mackinawite according to our DFT calculations.

TABLE 2: Derived Potentials for the Mackinawite Structure[a]

Buckingham potential	A (eV)	ρ (Å)	C (eV·Å^6)
Fe−S	1000.00	0.32	0.0
S−S	9201.82	0.3147	130.0
spring potential	K (eV·Å^{-2})		
S core − S shell	23.0		
ion charges	charge (e)		
Fe core	+2.000		
S core	+1.357		
S shell	−3.357		

[a] A cutoff of 15 Å is used for the Buckingham potentials.

parameters regardless of the level of electron correlation leaves only the nonmagnetic and ferromagnetic arrangements for the mackinawite structure. Our results show that the calculated

TABLE 3: Comparison of Potential Model and ab Initio Calculated Properties of an Isolated Layer of Mackinawite

	potential	ab initio
a, b (Å)	3.661	3.612
c (Å)	15.098	15.098
c_{11} (GPa)	48.6	46.9
c_{12} (GPa)	32.5	29.5
ν_1 (cm^{-1})	0.00	0.00
ν_2 (cm^{-1})	0.00	0.00
ν_3 (cm^{-1})	0.00	0.00
ν_4 (cm^{-1})	124	187
ν_5 (cm^{-1})	191	267
ν_6 (cm^{-1})	245	267
ν_7 (cm^{-1})	245	368
ν_8 (cm^{-1})	302	377
ν_9 (cm^{-1})	323	389
ν_{10} (cm^{-1})	323	397
ν_{11} (cm^{-1})	329	400
ν_{12} (cm^{-1})	413	414

relative stability of each is dependent upon the level of electron localization present. Low localization corresponds to a stable nonmagnetic state, whereas the ferromagnetic state is stable for higher values of correlation. Experimental evidence indicates that the mackinawite structure should be nonmagnetic,[6] and this case is indeed accurately simulated when $U_{eff} = 0$ eV. The lack of stability of this arrangement as the electron correlation is increased via the U_{eff} parameter indicates that mackinawite does not require an on-site term to account for electron correlation.

A clear picture of the conductive nature of the mackinawite structure is provided by the density of state (DOS) graphs for both the ferromagnetic and nonmagnetic cases (Figure 5), with the a parameter set to the internal energy minimum values given in Table 1 at all U_{eff} values under investigation. The Fermi energy is seen to cut a band of the Fe d orbital roughly in the

TABLE 4: Comparison of Calculated and Experimental Properties of Mackinawite[a]

	potential	experiment
a, b (Å)	3.667	3.674
c (Å)	5.033	5.033
c_{11} (GPa)	145.6	
c_{12} (GPa)	99.1	
c_{13} (GPa)	8.5	
c_{33} (GPa)	13.0	

[a] The c parameter was fixed at the experimentally determined value.

TABLE 5: Unrelaxed and Relaxed Surface Energies (J m^{-2}) for FeS

surface	100	010	001-S	001-Fe	110	101	011	111
$\gamma_{\text{unrelaxed}}$ (J m^{-2})	1.25	1.25	0.07	6.41	3.72	1.14	1.14	3.35
γ_{relaxed} (J m^{-2})	0.71	0.71	0.07	2.64	1.16	0.60	0.60	0.75

center of a local minimum, indicating the presence of mobile charge carriers, in agreement with the metallic nature deduced by Vaughan and Ridout.[6]

We also performed a series of total-energy calculations of the mackinawite structure to determine the total energy as a function of the lattice constant c. Setting the a and b lattice parameters to the experimentally verified values of 3.674 Å, the c parameter is varied between 3 and 20 Å. It is well-known that DFT-based calculations encounter difficulties when dispersive forces need to be taken into account.[45] Figure 6 indicates the difficulty experienced by DFT when predicting the interlayer distance, which does not show a clear minimum, where the experimentally confirmed value for c is denoted by the dashed line. In order to be able still to calculate relevant properties for the FeS layers, the interlayer distance will be increased 3-fold, thus removing any residual interactions between the layers. This procedure effectively converts the DFT calculation from a multilayer calculation into one for a single FeS layer, which for consistency will be adopted for the calculations of both the elastic constants and phonon modes which are then used in the derivation of a potential model.

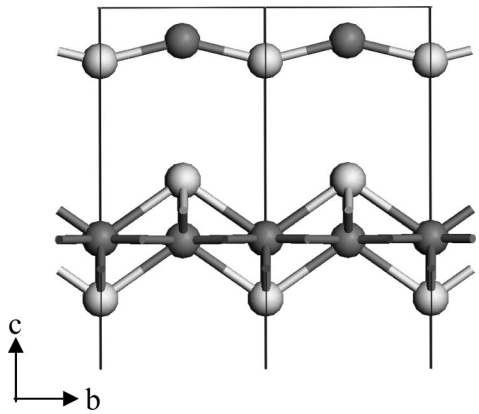

Figure 7. Schematic of the {001}-Fe surface, with a bulk layer beneath. (The iron atoms are colored dark gray, the sulfur atoms light gray. The lattice lines are provided to demarcate the surface and unit cell boundaries.) Viewed along the a-axis.

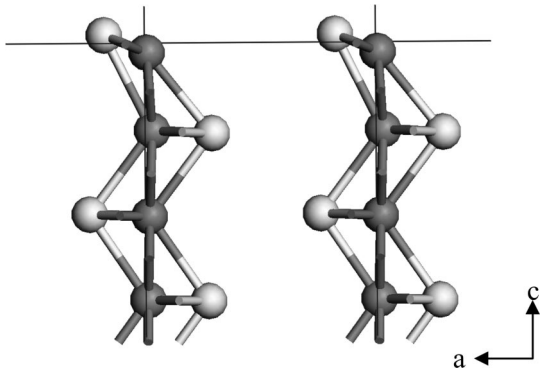

Figure 8. The relaxed surface structure of the {100} surface, viewed along the b-axis. (The iron atoms are colored dark gray, the sulfur atoms light gray. The lattice lines are provided to demarcate the surface and unit cell boundaries.)

Elastic constants relate an applied stress and the resultant strain upon a crystal lattice. Each elastic constant, c_{ij}, is defined as the second derivative of the energy density with respect to applicable strain components:

$$c_{ij} = \frac{1}{V}\frac{\partial^2 E}{\partial \varepsilon_i \, \partial \varepsilon_j}_0 \tag{1}$$

where V is the volume of the unit cell, E is the internal energy of the unit cell, and ε_i and ε_j are lattice strain components. Application of an appropriate stress tensor gives the following relation for the c_{11} constant:

$$c_{11} = \frac{1}{V}\frac{\partial^2 E}{\partial \varepsilon^2}_0 = \frac{2b}{V} \tag{2}$$

where b is the quadratic coefficient of a polynominal fit of E versus δ, where δ is the dimensionless strain ratio. Similarly,

$$c_{11} + c_{12} = \frac{b^*}{V} \tag{3}$$

where b^* is the c_{12} analogue of b.

Taking the case of $U_{\text{eff}} = 0$ eV and the nonmagnetic arrangement, by fixing the positions of the ions and measuring the energy density, the elastic constants may be found for the single FeS layer using a fitting procedure. Thus, c_{11} is determined according to eq 2 as

$$c_{11} = \frac{k_2}{V} = 46.9 \text{ GPa}$$

whereas c_{12} is given by eq 3 as

$$c_{12} = \frac{k_2}{V} - c_{11} = 29.5 \text{ GPa}$$

3.2. Interatomic Potential Parameters. The absence of experimentally confirmed, quantified physical data for mackinawite may account for the fact that to date no potential models have been derived for this structure. However, from the results of the DFT calculations in the previous section, it is now possible to fit interatomic potential parameters to the predicted elastic constants and phonon modes for the expanded-layer structure, listed in Table 2. The aim is to derive a set of interatomic potentials which successfully reproduces the structures and properties of both the expanded and experimental mackinawite structures.

Table 3 presents a comparison of the agreement between the properties from the ab initio calculations and the interatomic potential simulations of the single layer, whereas Table 4 lists the prediction of the structure and elastic constants of mackinawite, compared with experiment. The fitting to structural parameters for both the expanded layer and experimental structures is excellent, as is the fit to the elastic constants. The prediction by the ab initio methods of the conductivity of mackinawite suggests that within the Fe basal plane there is a degree of electron delocalization, which may be interpreted as

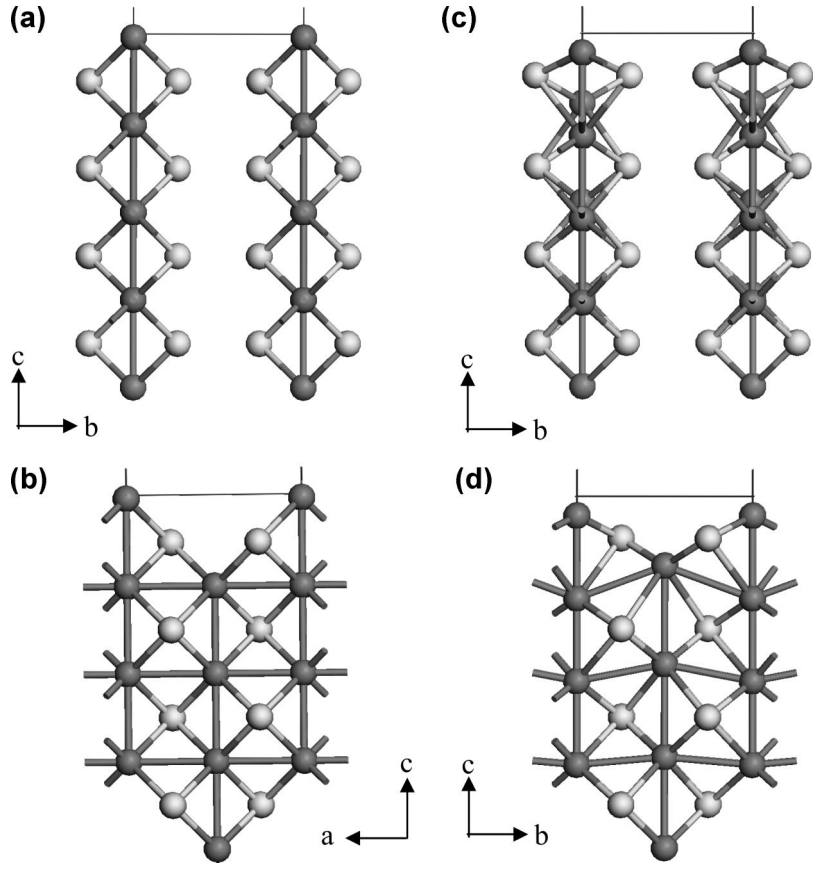

Figure 9. (a) Unrelaxed {110} structure viewed along the *a*-axis. (b) Unrelaxed {110} structure viewed along the *b*-axis. (c) Relaxed {110} structure viewed along the *a*-axis. (d) Relaxed {110} structure viewed along the *a*-axis.

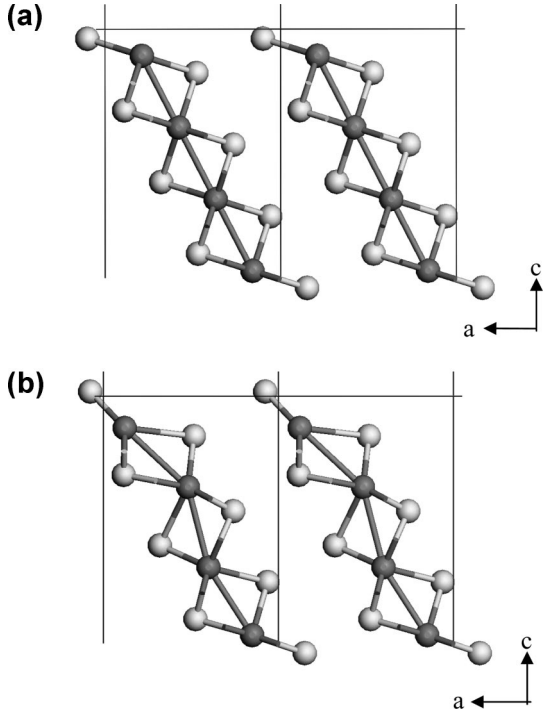

Figure 10. (a) Unrelaxed {111} structure viewed along the *b*-axis. (b) Relaxed {111} structure viewed along the *b*-axis.

a form of metallic bonding between the iron cations. This is not reproduced by the interatomic potential, which provides a possible explanation for the small discrepancies in elastic constants and phonon modes between the ab initio and interatomic potential calculations.

Figure 11. Calculated crystal morphology of mackinawite. The crystals grow in tabular forms, with the {001} surface highly prominent.

3.3. Surface Geometries and Energies. The simulated crystal structure was "cut" in a number of different directions to produce the {100}, {010}, {001}, {110}, {101}, {011}, and {111} surfaces of mackinawite.

The unrelaxed and relaxed surface energies are presented in Table 5. The symmetry of the crystal in the *a* and *b* directions leads to the equivalence of the {100} and {010} pair of surfaces, and also the {101} and {011} surfaces, which each possess only one unique repeat unit. The {001} surface possesses two distinct terminations where the {001}-S surface corresponds to a termination of the complete FeS layer, leaving a typical type II-terminated surface of S atoms (Figure 1), whereas the {001}-Fe surface is a reconstructed type III surface leaving a partially vacant layer of Fe atoms at the surface (Figure 7). The {011} surface possesses only a single repeat unit, but the {111} surface once again has two possible terminations, a type II and a reconstructed type III.

By far the most important surface in mackinawite is the {001}-S. Its very low surface energy is due to breaking only the weak interlayer van der Waal's S−S bonding between the S atoms, which results in only negligible relaxation of the surface species. The {001}-Fe termination divides the Fe−Fe basal plane into a reconstructed type III surface and as such breaks the greatest number of Fe−S bonds, leading to a high surface energy of 6.41 J m^{-2} prior to relaxation. Upon relaxation the surface atoms experience large displacements with the Fe−S

bond length decreasing from 2.24 to 1.89 Å and the Fe−S−Fe bond angle increasing from 110.0° to 152.8° (Figure 7).

The {100} and {010} surfaces also show a large reduction in the surface energy upon relaxation, of the order of 40%, with a displacement of the surface sulfur atom of 0.09 Å out of the plane of the surface (Figure 8). The next most stable surfaces are the {011} and {101}, which possess a surface energy of 0.60 J m^{-2} after relaxation, with a displacement of the surface Fe atom of 0.27 Å. Similarly, a very large relaxation is seen for the {110} surface, where a decrease in surface energy of 70% occurs upon minimization, whereas the {111} surface demonstrates an even larger decrease of 78%. These large reductions in surface energy upon relaxation demonstrate the relatively high instability of these surfaces and the requirement for a significant relocation of both S and Fe atoms at the surface. The {110} surface in particular demonstrates a notable reconstruction of the mackinawite structure upon relaxation (Figure 9a−d), as does the {111} surface (Figure 10, parts a and b).

Lennie et al.[11] performed electron diffraction experiments upon single crystals of approximately stoichiometric mackinawite and found patterns consistent with mackinawite lying with its {001} plane parallel to the carbon film substrate on which it was deposited, which to some extent confirms our finding that the {001} surface is the most chemically important surface in terms of crystal growth and the crystal morphology of mackinawite. The selected area electron diffraction (SAED) patterns obtained by Ohfuji and Rickard[46] of both freeze-dried and precipitated mackinawite show clearly the {001} as the most stable surface, followed in decreasing stability by the {101}, {200} (equivalent to the {100} surface), and {111} planes. These findings are in excellent agreement with the surface energies predicted by our derived potential model. The failure to experimentally observe the {110} surface reflections is explained by its relatively high surface energy, leading to this surface not arising in the calculated crystal morphology (Figure 11). The calculated crystal morphology is in excellent agreement with the crystals grown by Ohfuji and Rickard, who describe thin, tabular crystals. The lower than anticipated {111} surface reflection can be explained via its relatively higher surface energy compared to the {100} and {101} surfaces and its relative small contribution to the crystal morphology.

4. Conclusions

DFT calculations used to simulate the mackinawite structure have shown that the energetically most favorable stable solution is a metallic nonmagnetic state. The DOS calculations show that at all values for the U_{eff} parameter, the Fermi level of mackinawite cuts the Fe d orbital band, indicating the presence of mobile charge carriers in the plane of the mackinawite layers. In comparison with iron oxides, GGA predictions regarding mackinawite are accurate without a U_{eff} parameter, which is ascribed to the delocalization of the Fe 3d electrons. In more highly correlated materials the d electrons usually need to be localized by the U_{eff} parameter, but in mackinawite values other than $U_{eff} = 0$ eV give incorrect predictions of the magnetic nature. Rohrbach et al.[23] indicates three aspects of the GGA modeling of transition metal sulfides that are predicted incorrectly: semiconducting gap, too low magnetic moment, and too small an equilibrium volume. All these properties are improved by the inclusion of the Hubbard U_{eff} parameter. However, mackinawite is a nonmagnetic metallic compound with well-predicted lattice parameters, where inclusion of the changes associated with U_{eff} values would be incorrect.

The physical parameters predicted using a single-layer structure were utilized for the fitting of an interatomic potential, which predicts the elastic constants of the normal mackinawite structure to be $c_{11} = 145.6$, $c_{12} = 99.1$, $c_{13} = 8.5$, and $c_{31} = 13.0$. Calculations of both relaxed and unrelaxed surface energies has highlighted the stability of the {001} surface with S atom termination compared to all other surfaces, indicating that this surface is the most important in the crystal morphology. The calculated surface energies and resulting morphology are in excellent agreement with experimental findings regarding the most stable surfaces of synthetic crystals of mackinawite. Finally, the derived interatomic potential model is an excellent basis for future work on crystal growth and adsorption processes at the surfaces of mackinawite.

Acknowledgment. We thank the EPSRC for both financial support and use of the EPSRC's Chemical Database Service at Daresbury.

References and Notes

(1) Bertaut, E. F.; Burlet, P.; Chappert, J. *Solid State Commun.* **1965**, *3*, 335.
(2) Wolthers, M.; Charlet, L.; Van der Linde, P.R.; Rickard, D.; Van der Weuden, C. H. *Geochim. Cosmochim. Acta* **2005**, *69*, 3469.
(3) Watson, J. H. P.; Cressey, B. A.; Roberts, A. P.; Ellwood, D. C.; Charnock, J. M.; Soper, A. K. *J. Magn. Magn. Mater.* **2000**, *214*, 13.
(4) Livens, F. R.; Jones, M. J.; Moyes, L. N.; Pattrick, R. A. D.; Reed, W. A.; Vaughan, D. J.; Charnock, J. M.; Mosselmans, J. F. W.; Hennig, C. *Environ. Sci. Technol.* **2002**, *36*, 1757.
(5) Russell, M. J.; Hall, A. J. *J. Geol. Soc. (London)* **1997**, *154*, 377.
(6) Vaughan, D. J.; Ridout, M. S. *J. Inorg. Nucl. Chem.* **1971**, *33*, 741.
(7) Mullett, M.; Boursiquot, S.; Abdelmoula, M.; Génin, J.-M.; Ehrhardt, J.-J. *Geochim. Cosmochim. Acta* **2002**, *66*, 829.
(8) Kouvo, O.; Vuorelainen, Y.; Long, J. V. P. *Am. Mineral.* **1963**, *48*, 511.
(9) Lennie, A. R.; England, K. E. R.; Vaughan, D. J. *Am. Mineral.* **1995**, *80*, 960.
(10) Boursiquot, S.; Mullet, M.; Abdelmoula, M.; Génin, J.-M.; Ehrhardt, J.-J. *Phys. Chem. Miner.* **2001**, *28*, 600.
(11) Lennie, A. R.; Redfern, S. A. T.; Champness, P. E.; Stoddart, C. P.; Schofield, P. F.; Vaughan, D. J. *Am. Mineral.* **1997**, *82*, 302.
(12) Berner, R. A. *Am. J. Sci.* **1967**, *265*, 773.
(13) Muscat, J.; Hung, A.; Russo, S.; Yarovsky, I. *Phys. Rev. B* **2002**, *65*, 54107.
(14) de Leeuw, N. H.; Parker, S. C.; Sithole, H. M.; Ngoepe, P. E. *J. Phys. Chem. B* **2000**, *104*, 7969.
(15) Welz, D.; Rosenberg, M. *J. Phys. C: Solid State Phys.* **1987**, *20*, 3911.
(16) Taylor, L. A.; Finger, L. W. *Carnegie Inst. Washington Geophys. Lab. Annu. Rep.* **1970**, *69*, 318.
(17) Kresse, G.; Hafner, J. *Phys. Rev. B* **1993**, *47*, 558.
(18) Kresse, G.; Hafner, J. *Phys. Rev. B* **1994**, *49*, 14251.
(19) Kresse, G.; Furthmuller, J. *J. Comput. Mater. Sci.* **1996**, *47*, 558.
(20) Kresse, G.; Furthmuller, J. *Phys. Rev. B* **1996**, *54*, 11169.
(21) Payne, M. C.; Teter, M. P.; Allan, D. C.; Arias, T. A.; Joannopoulos, J. D. *Rev. Mod. Phys.* **1992**, *64*, 1045.
(22) Wells, S.; Alfe, D.; Blanchard, L.; Brodholt, J.; Calleja, M.; Catlow, R.; Price, D.; Tyler, R.; Wright, K. *Mol. Simul.* **2005**, *31*, 379.
(23) Rohrbach, A.; Hafner, J.; Kresse, G. *J. Phys.: Condens. Matter* **2003**, *15*, 979.
(24) Hobbs, D.; Hafner, J. *J. Phys.: Condens. Matter* **1999**, *11*, 8197.
(25) Marsella, L.; Fiorentini, V. *Phys. Rev. B* **2004**, *69*, 172103.
(26) Pinto, H. P.; Elliot, S. D. *J. Phys.: Condens. Matter* **2006**, *18*, 10427.
(27) Grau-Crespo, R.; Corà, F.; Sokol, A. A.; de Leeuw, N. H.; Catlow, C. R. A. *Phys. Rev. B* **2006**, *73*, 35116.
(28) Herper, H. C.; Hoffmann, E.; Entel, P. *Phys. Rev. B* **1999**, *60*, 3838.
(29) Perdew, J. P.; Chevary, J. A.; Vosko, S. H.; Jackson, K. A.; Pedersen, M. R.; Singh, D. J.; Fiolhais, C. *Phys. Rev. B* **1992**, *46*, 6671.
(30) Vosko, S. H.; Wilk, L.; Nusair, M. *Can. J. Phys.* **1980**, *58*, 1200.
(31) Blöchl, P. E. *Phys. Rev. B* **1994**, *50*, 17953.
(32) Kresse, G.; Joubert, D. *Phys. Rev. B* **1999**, *59*, 1758.
(33) Monkhorst, H. J.; Pack, J. D. *Phys. Rev. B* **1976**, *13*, 5188.
(34) Mermin, N. D. *Phys. Rev.* **1965**, *137*, A1141.
(35) Liechtenstein, A. I.; Anisimov, V. I.; Zaanen, J. *Phys. Rev. B* **1995**, *52*, 5467.
(36) Dudarev, S. L.; Botton, G. A.; Savrasov, S. Y.; Humphreys, C. J.; Sutton, A. P. *Phys. Rev. B* **1998**, *57*, 1505.
(37) Solovyev, I. V.; Dederichs, P. H.; Anisimov, V. I. *Phys. Rev. B* **1994**, *50*, 16861.
(38) Gale, J. D. *J. Chem. Soc., Faraday Trans.* **1997**, *93*, 629.

(39) Born, M. M.; Huang, K. *Dynamical Theory of Crystal Lattices*; Oxford University Press: Oxford, UK, 1954.
(40) Dick, B. G.; Overhausen, A. W. *Phys. Rev.* **1958**, *112*, 90.
(41) Watson, G. W.; Kelsey, E. T.; de Leeuw, N. H.; Harris, D. J.; Parker, S. C. *J. Chem. Soc., Faraday Trans.* **1996**, *92*, 433.
(42) Tasker, P. W. *J. Phys. C: Solid State Phys.* **1979**, *12*, 4977.
(43) Bertuat, F. *C. R. Acad. Sci.* **1958**, *246*, 3447.
(44) Wulff, G. *Z. Kristallogr.* **1901**, *34*, 499.
(45) Kristyán, S.; Pulay, P. *Chem. Phys. Lett.* **1994**, *229*, 175.
(46) Ohfuji, H.; Rickard, D. *Earth Planet. Sci. Lett.* **2006**, *241*, 227.

JP8001959